2009 American Control Conference
Hyatt Regency Riverfront, St. Louis, MO, USA
June 10-12, 2009

Motion Control of an Aerial Work Platform

QingHui Yuan, Jae Lew, Damrongrit Piyabongkarn

***Abstract*— An articulated aerial work platform is a type of off highway vehicle with a long/flexible beam to provide temporary access to inaccessable areas. The motivation of the research is to improve productivity and safety of the work platform via advanced control schemes. In this paper, a motion control architecture is presented for trajectory tracking and vibration suppression. By using the sensors integrated in hydraulic power elements, a closed loop coordinated control is presented to allow the end effector of the work platform to track a desired trajectory, thus alleviating the demand on operators' proficiency and improving productivity. In order to reduce the tracking error caused by the beam deflection, a Static Deflection Compensation Controller has been developed. In terms of vehicle safety, it has been observed that vibration associated with the long beam is significant, and the vibration characteristics change according to vehicle geometry. A unique input shaper is presented with the two impulses and the time varying parameters. The benefits are gaining robustness with respect to geometric variation, as well as reducing time delay for better responsiveness. The experimental study validates the controller.**

I. Introduction

An aerial work platform is a construction vehicle used to provide temporary access to inaccessible areas. There are several distinct types of platform for various applications. A scissor lift is one usually working only in vertical direction by using linked folding support in criss-cross X pattern. An articulated aerial work platform (AWP) is another type that consists of rotational and prismatic joints. The desired position can be reached by controlling the displacements of each joint. The articulated aerial work platform is widely used for maintenance and construction of a variety of industries, and even used as fire apparatus by fire fighters for high level access.

In this paper, we will focus on controlling an articulated aerial work platform with improved productivity and safety. An AWP includes multiple joints, each of which is driven by a linear or rotary actuator. Hydraulic cylinders and motors are widely used for such a system. In order to reach a desired position, an operator in the platform needs to use a joystick to control each actuator's speed separately. For such a type of "open loop" control method, some well-trained operators may be able to control multiple joints simultaneously to follow the intended trajectory in Cartesian space. However, the performance depends on operators' proficiency, and is hardly repeatable. By contrast, the closed loop coordinated control will use the sensors to measure a certain physical dimensions - very often the displacement of a hydraulic power element is measured due to the ease of assembly and integration. The orientation and coordinate of the end effector can be controlled accurately and repeatably to follow working trajectory, say the edge of a wall surface of a building. Therefore, the training time can be dramatically reduced, and the overall productivity will be increased.

Q Yuan, J Lew, and D Piyabongkarn are with Eaton Corp. Innovation Center, Eden Prairie, MN, USA. (Email: QinghuiYuan@Eaton.com, JaeYLew@eaton.com, NengPiyabongkarn@eaton.com)

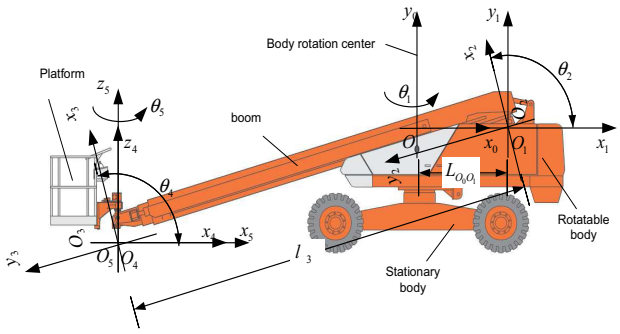

Fig. 1. Schematic and coordinate of aerial work platform

For such a long flexible structure with the human working on the platform, safety is a concern. One perspective of safety is associated with vibration. It has been observed that vibration associated with the long/flexilbe beam is significant and dangerous as the operational speed increases. Input shaping technique has proven its effectiveness of suppressing the vibration by generating the shaped command inputs. In the aerial work platform, we are particularly concerned with both robustness and responsiveness. In the past, it has been found that robustness to modeling errors can be improved by introducing the increased number of impulses [1]. However, robustness gained by the input shaping sequence with more impulses will be less responsive, which means more time delay [2]. For example, it will be not safe if the platform keeps moving if the operator has already commanded a stop. In this paper, we present a unique input shaping scheme whose control parameters are time varying so that it can reduce the vibration robustly across various geometric dimensions while maintaining good responsiveness, thus dramatically improving safety of the vehicle.

The paper is organized as follow. In section II, the overall system is described. Then, the motion control architecture and each essential functionalities are presented in section III. The experimental validation is presented in section IV. Finally, the concluding remarks are provided.

II. System Description

An aerial work platform, commercially available in the market, has been retrofitted. The platform has the maximum height of 24 [m], and the rated work load of 227 [Kg]. A schematic of such a vehicle can be seen in Fig. 1. In

a typical working cycle, the vehicle will be driven to the working space first, then the tire-to-tire width of the rear axis can be extended from 2.58 [m] to 3.80 [m] to stabilize the vehicle. In order to reach the work platform to any desired location, the combination of the following motions may be used. The vehicle body can rotate with respect to the center of rotation as denoted by θ_1. The motion is actuated by a hydraulic motor and a gear reducer. The beam is mounted on the rotatable vehicle body with a revolute joint, and can move upwards or downwards by the angle θ_2. The beam lift actuation is done via a hydraulic cylinder that is installed between the beam bottom and the vehicle body. The beam itself consists of three mechanical pieces: the base beam to connect the vehicle body, the intermediate beam, and the tip beam to connect the work platform. The length of the beam l_3 can be changed by retracting or extending the beams via a hydraulic cylinder and the corresponding mechanical linkage. A basket is mounted on the tip of the beam as a work platform for humans and additional loads. The pitch of the basket is always in parallel to the ground by a master-slave hydraulic system design, while the yaw orientation, as denoted by θ_5, is controlled by a hydraulic motor. In short, by controlling the hydraulic power elements aforementioned (motors and cylinders), the work platform can reach a desired location with a desired orientation within the work envelope.

During retrofitting, advanced mobile valves are installed to control the hydraulic power elements (Ultronics, Eaton, USA). Ultronics has the embedded pressure sensors and spool position sensors that enables energy saving [3] and accurate flow control. The flow control performance is achieved by robust spool position control like auto-tuning mechanism [4] and pressure compensation. This will dramatically simplify supervisory control development. Once the desired flow demand for each axis to the valve is generated from the supervisory control, the valve will ensure the accurate actual flow under varying operating conditions. The similar approach has been applied to a different type of vehicle (a wheelloader)[5].

Sensors are added to the original system to allow the closed loop control. Two laser sensors are utilized to measured the displacements of the lift cylinder and the extension cylinder. The rotation angles of hydraulic motors for the body swing and for the basket rotation are measured by two absolute angle encoders. Generally speaking, integrating the sensor into the hydraulic power elements are advantageous for the ease of assembly and integration.

III. Motion Control Development

In this section, we will formulate a motion control scheme with the focus on improving vehicle productivity and safety. The major objective is to achieve a smooth closed loop coordinated control. By considering all dominant disturbances observed in the vehicle operation, the control scheme is further decomposed to coordinated control, deflection compensation, axis control, and time varying input shaping, as illustrated in Fig. 2.

In this architecture, the trajectory generator (no shown) will generate the desired cartesian coordinate $X_d = [x_0, y_0, z_0, \phi_0]^T$ including both the position and the orientation of the end effector. Then a transformation function will convert X_d to Θ_d, the desired coordinate in a joint space. $\Theta_d = [\theta_1, \theta_2, l_3, \theta_5]^T$ as can be seen in Fig. 1. For a long flexible structure, deflection can cause a large error between the ideal end effector coordinate and the actual one. The error is a function of the coordinate - in different lifting height and length, deflection will be different. Deflection Compensation block will take the sensor measurement, and calculate the corresponding error correction in joint space, $\delta\Theta$. The resultant desired joint coordinate, Θ'_d, will be converted to one in the corresponding hydraulic power element space, Y_d. Here, $Y_d = [\theta_1, L_{AB}, l_3, \theta_5]^T$, which together with the actual power element displacement measurement Y_a, are fed to an axis control module to generate the control signal U for the flow control valve. As we mentioned, the advanced mobile valves allows us to send the flow rate demands directly to the valves instead of the spool position demand, which dramatically simplifies the high level control development. Finally, in order to reduce the structure vibration, a time varying input shaping scheme is developed to preshape the flow demand from U to U_s. Next, we will discuss each control module in details.

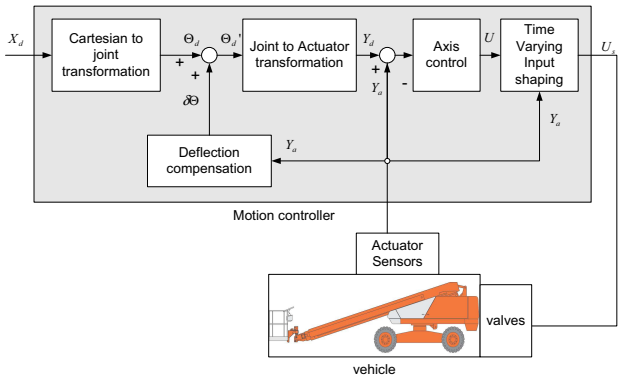

Fig. 2. Motion control architecture in which X_d is the desired Cartesian coordinate , Θ_0 the desired joint coordinate, $\delta\Theta$ the joint coordinate compensation for structure deflection, Θ'_d the desired joint coordinate after deflection compensation , Y_d the desired actuator space coordinate, Y_a the actual measurement, U the flow demand before input shaper, and U_s the flow demand after input shaper to be sent to the valves.

TABLE I
Relationship among Cartesian space, joint space, and actuator space

Cartesian space	Joint space	Actuator space
x^0	θ_1	θ_1
y^0	θ_2	L_{AB}
z^0	l_3	l_3
ϕ_0	θ_5	θ_5

A. Cartesian to Joint Transformation

Table I lists the independent variables among Cartesian space, joint space, and actuator space.

The forward transformation equation in the Cartesian coordinate is given by

$$X^{i-1} = T_i^{i-1} X^i \tag{1}$$

TABLE II

PARAMETER OF DENAVIT-HARTENBERG TRANSFORMATION FOR COORDINATES DEFINED IN FIG. 1

Joint number	a_i	θ_i	d_i	α_i
1	$L_{O_0O_1}$	θ_1	0	$+90^\circ$
2	0	θ_2	0	-90°
3	0	0	l_3	$+90^\circ$
4	0	θ_4	0	-90°
5	0	θ_5	0	0

where X^i is the position vector $[x^i, y^i, z^i, 1]^T$ in $O_i - x_i y_i z_i$

$$T_i^{i-1} = \begin{bmatrix} \cos\theta_i & -\sin\theta_i\cos\alpha_i & \sin\theta_i\sin\alpha_i & a\cos\theta_i \\ \sin\theta_i & \cos\theta_i\cos\alpha_i & -\cos\theta_i\sin\alpha_i & a_i sin\theta_i \\ 0 & \sin\alpha_i & \cos\alpha_i & d_i \\ 0 & 0 & 0 & 1 \end{bmatrix} \tag{2}$$

is the homogeneous transformation (position and orientation) of frame $O_i - x_i y_i z_i$ relative to the previous frame $O_{i-1} - x_{i-1}y_{i-1}z_{i-1}$ for $i = 1, \cdots, 5$. $T^{i-1}_{i,(1-3)\times(1-3)}$ are direction cosine of the coordinate axes of $O_i - x_i y_i z_i$ relative to $O_{i-1} - x_{i-1}y_{i-1}z_{i-1}$, and $T^{i-1}_{i,(1-3)\times(4)}$ is the position of O_{i-1} in $O_{i-1} - x_{i-1}y_{i-1}z_{i-1}$.

Note that in Eq. (2) the Denavit-Hartenberg notation is used to systematically describe the kinematic relationship where a_i is the length os the common normal, d_i is the distance between the original O_{i-1} and the intersect of the common normal to z_{i-1}, α_i is the angle between the joint axis z_i and z_{i-1} with respect to z_{i-1}, and θ_i is the angle between x_{i-1} and the common normal with respect to z_{i-1}. The parameters for the aerial platform are include in Table. II.

The resultant end-effector position and orientation can be obtained immediately by substituting the values of the joint displacements $\theta_1, \theta_2, l_3, \theta_4, \theta_5$. In this particular case, θ_4 is not an independent variable since $\theta_4 = \theta_2$ holds due to the hydraulic circuit design. So,

$$T_5^0 = T_1^0(\theta_1)T_2^1(\theta_2)T_3^2(l_3)T_4^3(\theta_2)T_5^4(\theta_5) \tag{3}$$

Once we have the end-effector position and orientation, we need to find the corresponding joint displacements to lead to the desired end effect position and orientation.

It is clear that forward transformation in Eq. (3) has the unique solution, while multiple solutions, on the other hand, may exist for the backward transformation[6]. We will solve the kinematic equation in Eq. (3) as follows.

Take the origin of $O_5 - x_5y_5z_5$, O_5, as an end effector. If the position of O_5 relative to $O_0 - x_0y_0z_0$ is $[x_0, y_0, z_0]^T$, and the angle between x_5 and x_0 is ϕ_0. We have a homogeneous transformation matrix of $O_5 - x_5y_5z_5$ in $O_0 - x_0y_0z_0$

$$T_5^0 = \begin{bmatrix} \cos\phi_0 & \sin\phi_0 & 0 & x_0 \\ \sin\phi_0 & -\cos\phi_0 & 0 & y_0 \\ 0 & 0 & 0 & z_0 \\ 0 & 0 & 0 & 1 \end{bmatrix} \tag{4}$$

Premultiplying both side of Eq. (3) by $T_1^0(\theta_1)^{-1}$ gives

$$T_1^0(\theta_1)^{-1}T_5^0 = T_2^1(\theta_2)T_3^2(l_3)T_4^3(\theta_2)T_5^4(\theta_5) \tag{5}$$

which actually represents O_5 in frame $O_1 - x_1y_1z_1$.

The left side of Eq. (5) and Eq. (4) yields

$$\begin{bmatrix} \cos\theta_1 & \sin\theta_1 & 0 & -L_{O_0O_1} \\ 0 & 0 & 1 & 0 \\ \sin\theta_1 & -\cos\theta_1 & 0 & 0 \\ 0 & 0 & 0 & 1 \end{bmatrix} \begin{bmatrix} \cos\phi_0 & \sin\phi_0 & 0 & x_0 \\ \sin\phi_0 & -\cos\phi_0 & 0 & y_0 \\ 0 & 0 & 0 & z_0 \\ 0 & 0 & 0 & 1 \end{bmatrix}$$
$$= \begin{bmatrix} \cos\theta_1\cos\phi_0 + \sin\theta_1\sin\phi_0 & * & * & x_0\cos\theta_1 + y_0\sin\theta_1 - L_{O_0O_1} \\ * & * & * & z_0 \\ * & * & * & x_0\sin\theta_1 - y_0\cos\theta_1 \\ * & * & * & * \end{bmatrix} \tag{6}$$

The right side of Eq. (5) yields

$$\begin{bmatrix} \cos\theta_5 & * & * & -l_3\sin\theta_2 \\ * & * & * & l_3\cos\theta_2 \\ * & * & * & 0 \\ * & * & * & * \end{bmatrix} \tag{7}$$

Four equations can be formulated from Eq. (6) (7) to solve the four joint displacements

$$\Theta(X) := \begin{bmatrix} \theta_1 \\ \theta_2 \\ l_3 \\ \theta_5 \end{bmatrix} = \begin{bmatrix} \arctan\left(\frac{y_0}{x_0}\right) \\ \arctan\left(\frac{L_{O_0O_1} - x_0\cos\theta_1 - y_0\sin\theta_1}{z_0}\right) \\ \frac{z_0}{\cos\theta_2} \\ \phi - \theta_1 \end{bmatrix} \tag{8}$$

that gives the Cartesian-to-joint transformation.

B. Static Deflection Compensation

The deflection of the long beam causes the end effect coordinate tracking error in Cartesian space. As illustrated in Fig. 3, the error mainly comes from θ_2. For the rest of the degree of freedom, the errors are negligibly small. Then the compensation vector can be defined as

$$\delta\Theta = [0, \delta\theta_2, 0, 0]^T$$

Next, we will formulate the equation to predict the errors based on the vehicle orientation.

In Fig. 3, the deflection of the beam is contributed by the gravity of the beam and the load in the aerial platform in the tip, as a functions of the beam length l_3 and the beam rotation angle θ_2. By assuming that the uniformly distributed cross section of the beam, we have

$$\delta(l_3, \theta_2) = \left(\frac{mgl_3^3}{3EI} + \frac{\rho g l_3^4}{8EI}\right)\sin\theta_2 \tag{9}$$

where E is the modulus of elasticity of the beam material, I is the moment of inertia of the cross section, ρ is the mass length density, m is the mass of the load.

Equivalently, a rigid beam with the rotation angle θ_2' can have the same tip position if $\delta\theta_2 := \theta_2' - \theta$ is given by

$$\delta\theta_2(l_3, \theta_2) = \frac{\delta(l_3, \theta_2)}{l_3} = \left(\frac{mgl_3^2}{3EI} + \frac{\rho g l_3^3}{8EI}\right)\sin\theta_2 \tag{10}$$

where l_3, θ_2 are calculated from the actual measurement Y_a is in the actuator space.

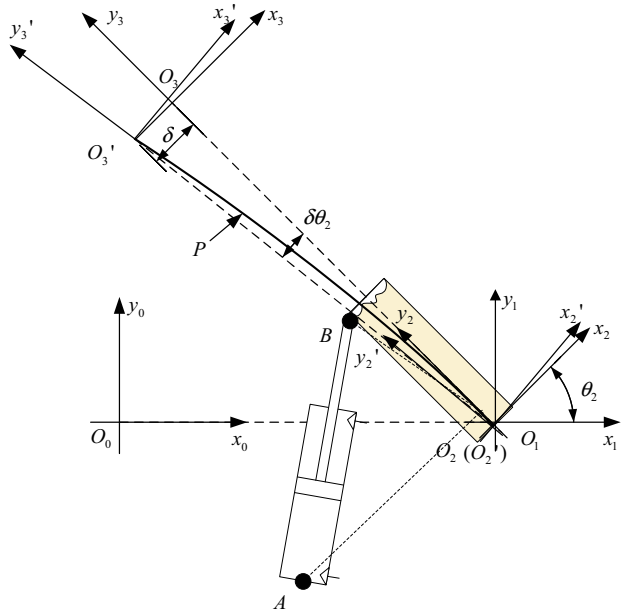

Fig. 3. Joint-actuator space transformation

C. Joint to Actuator Space Transformation

Actuator space refers to either hydraulic cylinder or hydraulic motor. Table I lists the independent variables among Cartesian space, joint space, and actuator space. Obviously, the relationship between joint space and actuator space is very straightforward except $\theta_2 - L_{AB}$ pair.

In Fig. 3, the schematic of beam cylinder mounting is described. A hydraulic double acting cylinder is mounted between A and B where A is a fixed point in the vehicle body frame ($O_1 - x_1y_1z_1$), and B is fixed at beam ($O_2 - x_2y_2z_2$). We have

$$l_{AB}(\theta_2) = \sqrt{L_{BO_1}^2 + L_{AO_1}^2 - 2L_{AO_1}L_{BO_1}\cos\angle BO_1A(\theta_2)} \tag{11}$$

where $\angle BO_1A(\theta_2) = 90^\circ + \angle O_0O_1A - \theta_2 - \angle BO_1O_3$

Then we have the joint to actuator space transformation as below

$$Y(\Theta) := \begin{bmatrix} \theta_1 & l_{AB}(\theta_2) & l_3 & \theta_5 \end{bmatrix}^T \tag{12}$$

D. Axis control

The joint to actuator transformation decomposes the desired trajectory for each hydraulic power element. The axis control can be developed for each actuator separately. A simple velocity feedforward PI controller could be

$$q_n = K_{f,n}\dot{y}_{d,n} + K_{p,n}(y_{d,n} - y_{a,n}) + K_{i,n}\int(y_d - y_a)dt \tag{13}$$

where q_n is the flow command for valve n, $K_{f,n}, K_{p,n}, K_{i,n}$ is the feedforward, proportional, and integral gains, respectively, and $y_{d,n}, y_{a,n}$ are the desired and actual displacement for axis number $n = 1, 2, \cdots, 4$. Note that for the hydraulic cylinder, the gains will be slightly different for each direction due to piston area ratio.

The flow command vector generated by the axis control block is given by

$$U = [q_1, q_2, q_3, q_4]^T$$

Since the advanced mobile valve has the embedded sensors and inner loop control, the axis control development has been dramatically simplified.

E. Time varying Input Shaping

In order to minimize the time delay, we choose the input shaping method with two impulses, or Zero Vibration (ZV) shaper. However, such a control scheme is very sensitive to modeling errors [2]. Instead of taking the approach like Zero Vibration and Derivative (ZVD) [1] by adding more impulses, we would like to utilize the measurement signals available in the vehicle to develop an input shaper whose parameters are time varying so that the optimal performance can be achieved all the time.

The algorithm is presented as follow. First, estimate the damping ratio and the natural frequency of the structure based on the measurement Y_a.

$$\begin{aligned} \zeta(t) &= f_\zeta(Y_a) = f_\zeta(l_3(t)) \\ \omega_n(t) &= f_\omega(Y_a) = f_\omega(l_3(t)) \end{aligned} \tag{14}$$

where f_ζ and f_ω can be determined from modeling or experimental calibration, with the assumption that l_3 is the only dominant variable among all the measured, and the effect from payload is negligibly small.

Then, the amplitudes of two impulse are given by

$$A_1(t) = \frac{1}{1 + K(t)} \tag{15}$$

$$A_2(t) = \frac{K(t)}{1 + K(t)} \tag{16}$$

where $K(t) = \exp\left(\frac{\zeta(t)\pi}{\sqrt{1-\zeta(t)^2}}\right)$

The time delay for each impulse is

$$\Delta T_1(t) = 0 \tag{17}$$

$$\Delta T_2(t) = \frac{\pi}{\omega_n(t)\sqrt{1 - \zeta(t)^2}} \tag{18}$$

Finally, the flow command U_s after the input shaper is

$$U_s = \begin{bmatrix} q_1 \\ A_1(t)U_2(t - \Delta T_1(t)) + A_2(t)U_2(t - \Delta T_2(t)) \\ q_3 \\ q_4 \end{bmatrix} \tag{19}$$

IV. Experimental Study

Fig. 4 shows the retrofitted aerial work platform. We replace the original valves with the Ultronics valves (Eaton, USA) to enable the direct flow control with pressure compensation. The valves exchange the information with the Mototron ECU (MotoTron, USA) through a CAN bus. The motion control algorithm is compiled and downloaded to the ECU via Matlab and MotoHawk toolchains. The software

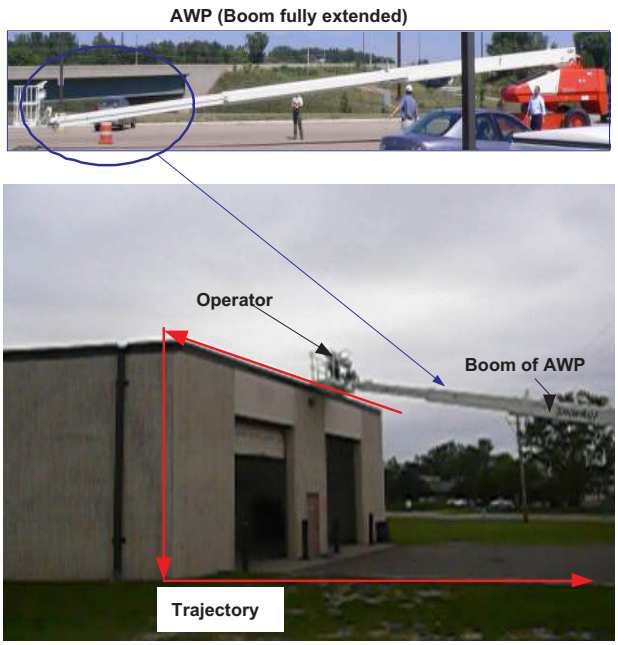

Fig. 4. The retrofitted AWP and experimental validation process.

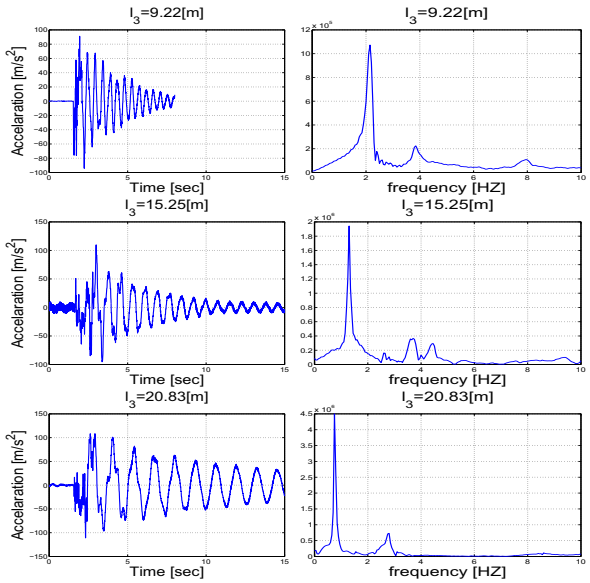

Fig. 5. The recorded experimental data for accelerometer responses (left) and their corresponding frequency spectra. The figures shows the data for three beam lengths: l_3 = 9.22 15.25 20.83 [m] from top to bottom.

in the ECU is responsible for collecting the sensor signals, computing the flow demands via the complex control algorithm described in Section III, and finally sending the flow rate demands to the valves. The joystick in the basket can be configured to switch between the open loop mode, in which the joystick directly send the flow demand to each actuator based on the joystick position, and the closed loop mode, in which the desired trajectory in Cartesian space can be defined from the initial coordinate when the closed loop mode is enabled, and the velocity in each coordinate set by the joystick positions.

The overall closed loop tracking performance in Cartesian coordinate is validated experimentally. Since it is not easy to directly measure the coordinate of the end effort, we actually select a cuboid shaped building as a reference. The AWP is parked in an appropriate distance to the building, then the end effector is commanded by the operator to follow the edges of the building in the different coordinate, as shown in Fig. 4. The tracking trajectory is demonstrated by projecting a point of light from a laser pointer mounted on the basket to the references. The maximum error in the entire trajectory, which has been defined to cover the entire work envelope (the beam with the maximum length of 24 [m]), is less than 0.1 [m]. It is also observed in the study that without Static Deflection Compensation control, the maximum tracking error will increase up to 0.6 [m], in the case as the beam is fully extended. Since the input shaping control significantly suppresses the vibration in beaming mode as discussed below, the proposed Static Deflection Compensation method has been proved to be valid.

In the rest of this section, we will focus on validating the time varying input shaping method. Since there is no sensor on the end effector, the vibration generated in the long beam can not be captured by the sensors mounted on the hydraulic power elements. Therefore, an extra accelerometer is introduced to the system. The accelerometer is attached on the tip of the platform. An operator intentionally injects vibration to the beam by commanding an abrupt motion maneuver via the joystick. During the vibration, the acceleration signals are recorded.

The time responses and their frequency spectra for various beam lengths are measured and calculated, respectively. Three of them are shown in Fig. 5. We have

- There is a single dominant mode for all cases. This implies that our time varying input shaper with two impulses is a valid solution (See [7] [8] for multiple modes solutions).
- The frequency of the dominant mode decreases as the beam length l_3 increases.
- Non-dominant modes show complex pattern, which may be related to the irregular three pieces constructed beam.

The calibrated parameters for the time varying input shaping $f_\zeta(\cdot)$ and $f_\omega(\cdot)$ are plotted in Fig. 6. Obviously, both the natural frequency and the damping ratio are the functions of l_3. As the beam length increases, the natural frequency goes down, so does the damping ratio. The model variation is significant. When the beam is fully extended, the natural frequency is only 35% of that for fully retracted beam.

The effectiveness of the time varying input shaping has been demonstrated in the following comparison study. In addition to the proposed time varying input shaper, a conventional ZV input shaper [1] is also implemented by assuming a set of constant values: $\zeta = 0.026$ and $\omega = 9.2$ [rad/s], which corresponds to the physical property as the beam is half extended. During the testing, the beam is extended to a certain length. The operator introduces a vibration

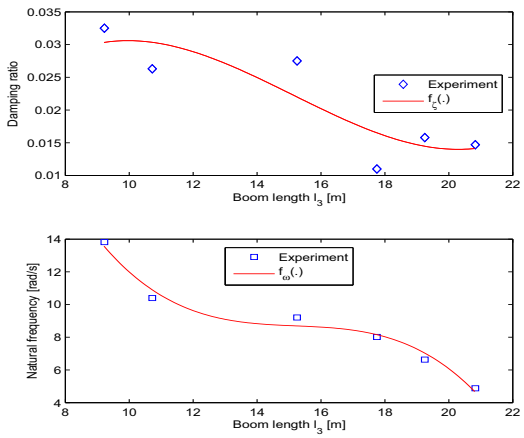

Fig. 6. The calculated damping ratio and the natural frequency for various beam length, and the calibrated $f_\zeta(\cdot)$ and $f_\omega(\cdot)$.

to the beam in the same manner as before by using the joystick. We record the accelerometer responses for two types of input shapers. The cases where the input shapers are disabled are also considered for the sake of comparison. In Fig. 7, the responses are illustrated for $l_3 = 9.5$, 15, and 19 [m], respectively. In all the cases, the system with the input shapers will stabilize faster than the one without any input shaper. Due to the wide range of variation of physical properties, the conventional ZV input shaping only demonstrates the comparable performance as the beam is in the middle (close to the nominal value selected). Under the other conditions, more significant vibration has been observed. The time varying input shaping provides the great performance and robustness in the entire range of the beam motion range. In addition, the time varying input shaper has the comparable responsiveness as the ZV input shaper, as shown in the figure.

V. Conclusion

The research addresses productivity and safety of the aerial work platform via advanced control scheme. In this paper, a closed loop coordinated control is presented to allow the end effector of the work platform to track a trajectory in Cartesian coordinate, thus reducing the demands on operators' proficiency and improving productivity. A Static Deflection Compensation method has been developed for further reducing the tracking error caused by the beam deflection. In terms of vehicle safety, it has been observed that vibration associated with the long/flexible beam is significant and dangerous. A time varying input shaping technology is presented with both robustness to the vehicle geometric variation and responsiveness to operators' command. The proposed controller has been implemented on an retrofitted aerial work platform. Accurate tracking and suppressed vibration have been validated in experiment.

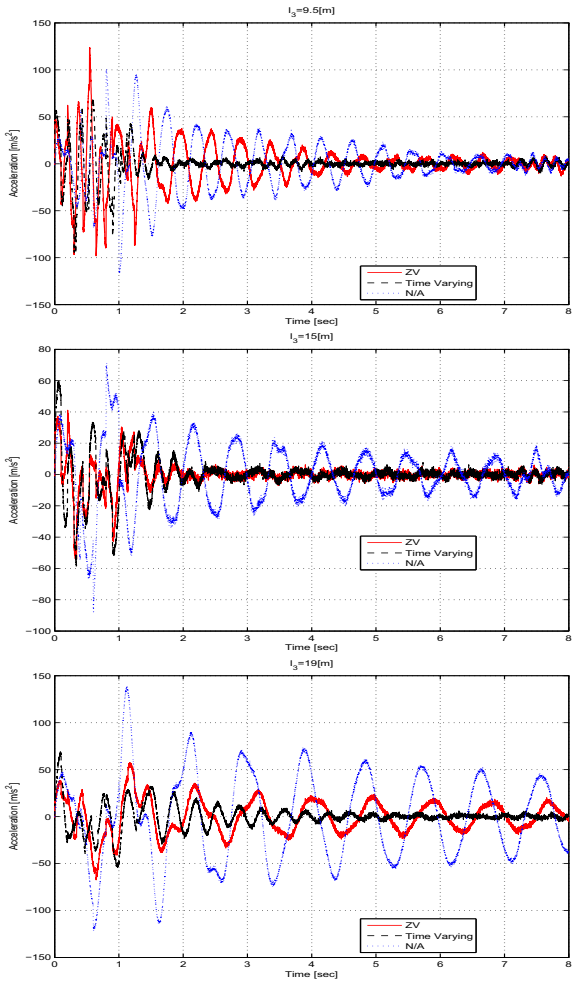

Fig. 7. Experimental results for a conventional ZV input shaping method and the proposed time varying input shaping. "N/A" represents the case where no input shaping has been implemented.

References

[1] N. C. Singer and W. P. Seering, "Preshaping command inputs to reduce system vibration," *ASME Journal of Dynamic Systems, Measurement, and Control*, vol. 112, no. 1, pp. 76–82, Mar 1990.

[2] T. Singh and W. Singhose, "Tutorial on input shaping/time delay control of maneuvering flexible structures," in *The 2002 American Control Conference*, Anchorage, AK, May 2002, pp. 1717–1731.

[3] Q. Yuan and J. Y. Lew, "Modeling and control of a two-stage twin-spool valve for energy-saving," in *the 2005 American Control Conference (ACC)*, vol. 6, Portland, OR, Jun 2005, pp. 4364–68.

[4] Q. Yuan, "A model free automatic tuning method for a restricted structured controller by using simultaneous perturbation stochastic approximation (spsa)," in *The 2008 American Control Conference*, Seattle, WA, June 2008.

[5] Q. Yuan, S. Bengea, D. Piyabongkarn, and P. Brenner, "Dynamic control of a distributed embedded eletro-hydraulic system," *SAE 2007 Transactions Journal of Passenger Cars: Electronics and Electrical Systems*, vol. 2007-01-1626, Aug. 2008.

[6] H. Asada and J.-J. E. Slotine, *Robot Analysis and Control*. Wiley-Interscience, Apr. 1986.

[7] D. Magee and W. Book, "Eliminating multiple modes of vibration in a flexible manipulator," in *IEEE International Conference on Robotics and Automation*, vol. 2, May 1993, pp. 474–479.

[8] W. Singhose, D. Kim, and M. Kenison, "Input shaping control of double-pendulum bridge crane oscillations," *ASME Journal of Dynamic Systems, Measurement, and Control*, vol. 130, no. 3, p. 034504, May 2008.